ARTICLE

Linking the Cu(II/I) and the Ni(IV/II) Potentials to Subsequent Passive Film Breakdown for a Cu-Ni Alloy in Aqueous 0.5 M NaCl

Amelia R. Langley,[a]* Aisling Elmer[a], Philip J. Fletcher[b] and Frank Marken[a]*

Abstract: Copper and copper-nickel alloys are known to form partially passive films in marine conditions, both naturally and under positive potential bias. Here, the anodic passivation behaviour of copper and of constantan (Cu54Ni45Mn1) as a model for a copper-nickel alloy are investigated and compared at high positive overpotentials and in 0.5 M NaCl(aq). Abrupt potential-dependent passive film breakdown is observed for both Cu and Cu-Ni alloys during voltammetry and during chrono-amperometry experiments. For Cu a single transitions occurs at 0.2 V vs. SCE consistent with a Cu(II/I) process leading to interfacial stress and breaking of a passive CuCl film. For Cu-Ni alloy, two stages are observed at 0.3 V *vs.* SCE due to a Cu(II/I) process and at 1.7 V *vs.* SCE due to a sub-interfacial Ni(IV/II) process. A breakdown mechanism is proposed based on redox processes at the buried interface at the metallic conductor | passive ion conductor junction.

Introduction

A large variety of metals are used within the marine industry. The harsh marine environment leads to severe corrosion issues; thus research is geared heavily towards the prevention of corrosion via routes such as cathodic protection (for steel pipelines),[1–3] and using protective coatings.[4–6] One alternative form of protective coating can be based on passive films, generated anodically to protect the underlying metal from further corrosion.[7–9] These passive films block a wide range of redox processes, but also show potential dependent break down phenomena. Characteristic voltammetric signatures can be observed at positive applied potentials beyond those usually applied in aqueous environments.

Here, (partially) passive films are investigated for copper and the copper-nickel alloy constantan (formally Cu54Ni45Mn1). Without the presence of electrochemical stimuli, copper in seawater forms relatively stable copper oxide and chloride layers over time in the presence of O_2.[10–13] Passive films can also be formed electrochemically by applying a positive bias to copper in pH neutral seawater, where cuprous chloride (CuCl) is the predominant corrosion product (equation 1).[10,14–16]

$$Cu(s) + Cl^-(aq) \rightleftharpoons CuCl(s) + e^- \quad (1)$$

Alloying of metals usually leads to improved corrosion resistance of otherwise susceptible metals. Prominent examples are alloying steel with chromium or manganese,[17] and copper with nickel.[18–20] An alloy with composition Cu90/Ni10 shows improved corrosion resistance in a marine environments.[10,21,22] Copper-nickel alloys are widely used in the marine industry in, for example, desalination plants, pipework, and pumps.[18] The improved corrosion resistance of copper-nickel alloys is known to be a result of a passive film containing nickel-rich oxides.[23–28] Passive films, however, are susceptible to breakdown. The potential-driven breakdown of passive films is compared here for small electrodes made from Cu and Cu54Ni45Mn1.

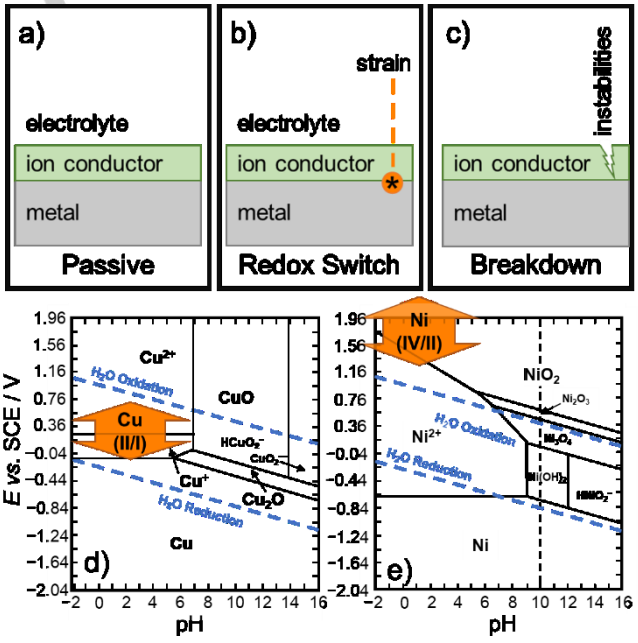

Figure 1. *Schematic drawing of the metal | ion conductor | electrolyte interface in the a) passive state, b) with strain represented at the metal | ion condutor interface due to a Cu(II/I) or Ni(IV/II) redox process and c) subsequent breakdown of the passive film due to strain. E-pH plots (Pourbaix diagrams[37]) simplified and scaled to SCE for d) copper and e) nickel in water. Arrows indicate the formation of strain at Cu(II/I) or Ni(IV/II) potentials.*

The breakdown of a passive film generally occurs due to mechanical and chemical changes. Lohrengel and Schultze[29] provide a summary of passive film breakdown causes, which include dielectric breakdown,[30,31] and Cl^- ion anion penetration

[a] Amelia R. Langley, Aisling Elmer and Prof. Frank Marken
Department of Chemistry
University of Bath
Claverton Down, Bath BA2 7AY
E-mail: A.R.Langley@bath.ac.uk, F.Marken@bath.ac.uk
[b] Dr. Philip J. Fletcher
Materials and Chemical Characterisation Facility MC^2,
University of Bath
Claverton Down, Bath BA2 7AY

(leading to pitting and localized dissolution and corrosion).[32,33] Additional pathways for breakdown could be linked to redox-induced strain within the passive interfacial layer.[34] This could be caused by redox processes in the solid state at the metal | ion conductor interface or also due to the redox induced formation of traces of gaseous species. The nature of the passive film generally dictates the breakdown pathway, which can cause, for example, phenomena such as pitting.[35,36] Passive film stability depends on a variety of factors including solubility, pH and interfacial reactivity in a given environment. In a recent study for copper, it has been shown that also electrode diameter and the nature of the gaseous species dissolved in the solution phase can affect breakdown of passive films.[34] This directly implied for the Cu | CuCl system in aqueous 0.5 M chloride solution the absence of anodic gas evolution processes (oxygen or chlorine) even at high positive applied potentials.

To explore changes in passive film stability, voltammetry experiments can be employed to explore changes in mechanism as a function of applied potential. Figure 1a-c shows a diagram schematically depicting a metal | passive film | electrolyte interface assuming some degree of ion conductivity through the passive film (or through the grain boundaries present in this material). The schematic shows a passive film breakdown mechanism linked to redox-induced strain at the metal | ion conductor interface. Such strain is suggested here to be linked to sub-interfacial inter-layer redox processes involving Cu or Ni (see Figure 1).

In this work, anodic pitting and the breakdown of passive films formed on a copper-nickel alloy (constantan) are investigated in model seawater.[38–42] A mechanism based on strain due to oxidized copper and nickel species and subsequent reactions at the metal | passive film interface is proposed. Redox processes responsible for the strain are identified by comparison of data from voltammetry to data in Pourbaix diagrams (see Figure 1).

Results and Discussion

Linear sweep voltammetry at a scan rate of 5 mV s^{-1} was conducted from equilibrium to high potentials (+5 V *vs.* SCE) to investigate passive film formation and behaviour. Microelectrodes based on 125 µm diameter wire were prepared for pure copper, constantan (Cu54Ni45Mn1), and pure nickel (see experimental). Figure 2a depicts a typical linear sweep voltammogram obtained with a scan rate of 5 mV s^{-1} for a pure copper 125 µm diameter electrode immersed in aqueous 0.5 M NaCl. An initial anodic peak at approx. −0.11 V *vs.* SCE is observed associated with the formation of CuCl (see equation 1). The thickness of this passive film has been reported to be typically 0.4 µm.[15] A second anodic peak is observed at approx. +0.2 V *vs.* SCE. Immediately following this anodic peak at +0.2 V *vs.* SCE for pure copper, characteristic current noise is observed. The second anodic peak and commencement of current noise have been linked to sub-interfacial Cu(II) formation at the Cu | CuCl interface causing instabilities in the passive film.[15] Current spikes are also observed (up to 40 µA in magnitude), representing CuCl film breakdown and colloidal dissolution events of the CuCl film.[15] This process has been shown to be dependent on the presence of dissolved gases in the solution phase, probably due to gas bubble nucleation and implosion during breakdown.[34] The Cu(II/I) redox transition (see Figure 2a) produces current associated with copper dissolution relatively uniformly with some spikes up to +5 V vs. SCE applied potentials.

Voltammetric current traces for a 125 µm diameter constantan electrode (see Figure 2b-c) exhibit similar characteristics to those observed for pure copper. An initial anodic current peak is observed at a potential of approx. 0.1 V *vs.* SCE. The anodic peak current increases from 10 µA for pure copper, to 20 µA for constantan. The increased anodic peak current could be due to the additional dissolution of nickel as highly soluble Ni^{2+} (see equation 2) simultaneous to the formation of insoluble CuCl (see equation 1) passivating the surface.

$$Ni(s) + 2Cl^-(aq) \rightleftharpoons NiCl_2(aq) + 2e^- \quad \textbf{(2)}$$

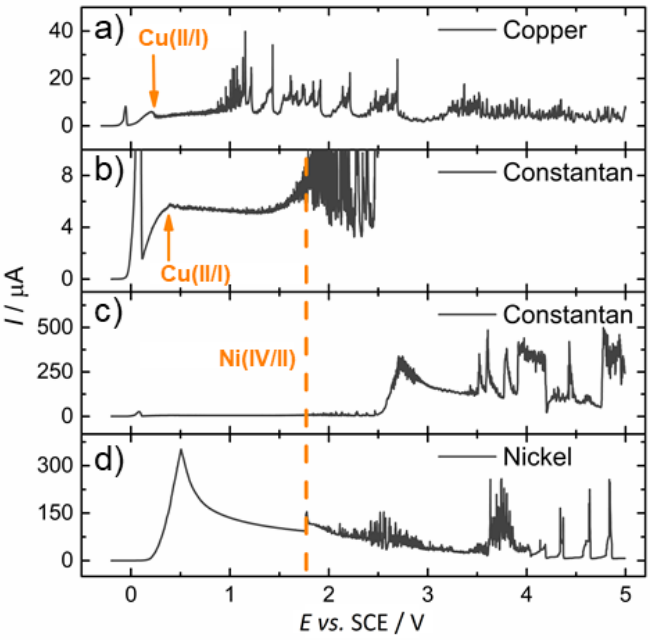

Figure 2. *Linear sweep voltammograms for a) pure copper, b-c) constantan (Cu54Ni45Mn1) d) pure nickel 125 µm diameter microelectrodes immersed in 0.5 M NaCl(aq) at 5 mV s^{-1} from approx. −0.25 V to +5.0 vs. SCE. Cu(II/I) redox switch is indicated in a) and b), and the Ni(IV/II) indicated (orange dashed line) for b-d) at approx. 1.8 V vs. SCE.*

At approx. +0.3 V *vs.* SCE for constantan the onset of noise in the voltammogram can be linked to the Cu(II/I) redox process at the metal | passive film interface causing strain (see Figure 1). The currents in the potential region from 0.1-1.8 V *vs.* SCE (see Figure 2b) remain relatively low (typically 5-6 µA, see Table 1) consistent with a partially passive region, but similar to those for pure copper. At a potential of 1.7 or 1.8 V *vs.* SCE the

voltammetric response for constantan changes considerably compared to pure copper, with an increase in current noise and an apparent catastrophic breakdown at 2.5 V vs. SCE (see Figure 2c). For comparison, voltammetric signals for a pure nickel electrode are shown in Figure 2d. A large anodic peak at 0.5 V *vs.* SCE is attributed to the rapid dissolution of highly soluble Ni^{2+} in aqueous media (equation 2).[37,43] Following this, a relatively high current is maintained throughout the higher potential range for pure nickel, including a transition to current noise at approximately 1.7 or 1.8 V *vs.* SCE.

Table 1. *Passivation current data (in the range 0.5 to 1.5 V vs. SCE) measured from voltammograms at 125 µm diameter copper, constantan, and nickel electrodes (see Figure 2) in 0.5 M NaCl(aq).*

Metal	$I_{passivation}$[a] / µA
Cu	5-6
Cu54Ni45Mn1	5-6
Ni	100

[a] passivation current approximated from the current noise baseline for pure copper and nickel, see Figure 2.

To investigate the initial formation of a passive film at lower potentials, cyclic voltammetry was employed, limited to 0.3 V *vs.* SCE for copper and constantan. Figure 3a shows the first cyclic voltammogram for a pure copper 125 µm diameter electrode. Two anodic peaks are observed. The first anodic peak at 0.0 V *vs.* SCE is attributed to CuCl formation (equation 1).[15,34] The second anodic peak at approx. 0.2 V *vs.* SCE is attributed to the formation of Cu(II) causing strain in the passive film and leading to instabilities observed as current noise thereafter (see Figure 1a-c).[15,34] For constantan, only one anodic peak is observed at approx. 0.2 V *vs.* SCE during the first cycle (see Figure 3b). This anodic peak is attributed to the concomittant dissoluton of Ni as Ni^{2+} (equation 2) and the formation of CuCl and subsequent passivation of the alloy surface. For anodic peaks observed for copper and constantan during the first cycle (Figure 3a-b respectively), the anodic peak currents increase with increasing scan rate. Cathodic peaks for CuCl reduction are observed at -0.2 V vs. SCE, but only at a higher scan rate due to competition with diffusional losses of CuCl.

During the second potential cycle for constantan (see Figure 3c), a new anodic peak at approx. 0.0 V *vs.* SCE is observed (in addition to the anodic peak at 0.2 V *vs.* SCE). The first anodic peak correlates well with the CuCl formation at 0.0 V *vs.* SCE, similar to the process observed for copper (Figure 3a). The anodic peak currents for both peaks are considerably smaller (< 30 µA) than the currents obtained in the first cycle (up to 80 µA). The appearance of a CuCl peak at 0.0 V *vs.* SCE during the second cycle could be due to the removal of surface nickel at the electrode surface during the first cycle and the re-deposition of pure copper onto constantan. The anodic peak at 0.0 V *vs.* SCE for constantan (second cycle, Figure 3c) depends on the scan rate, becoming more prominent at slow scan rates. This could be explained by there being more time for Cu(I) to reduce to Cu(0) at 5 mV s^{-1} during the first cycle (see Figure 3c). The shift in onset potential for oxidation for pure copper (peak i) to that for constantan (peak ii) is likely to be associated with alloying (see XRD data in Figure SI1) and linked to the lower rate of corrosion of constantan. The role of Mn in the electrochemical behaviour is assumed here to be relatively minor.

Next, cyclic voltammetry was performed to +3.0 V *vs.* SCE for constantan to investigate the high current noise transition observed at approx. 1.7 V *vs.* SCE during linear sweep voltammetry (see Figure 3d). The cyclic voltammogram to 3 V *vs.* SCE for constantan shows the high current noise ceasing between 1.5-2.0 V *vs.* SCE during the reverse scan.

It is interesting to interpret the voltammetric features observed for constantan in terms of characteristic redox processes at the metal | passive layer | electrolyte interface. The onset of noise at approximately 0.2 V vs. SCE for both copper and constantan (see below) has been assigned to strain caused by Cu(II/I) (see Figure 2a-b). At 1.7 V *vs.* SCE, additional noise and an increase in current are observed, and then at 2.5 V vs. SCE an order of magnitude increase in current occurs (up to 500 µA). The corresponding passive film breakdown is assigned here to a Ni(IV/II) redox process at the metal | passive film interface, consistent with a transition suggested in the Pourbaix diagrams (see Figure 1e).

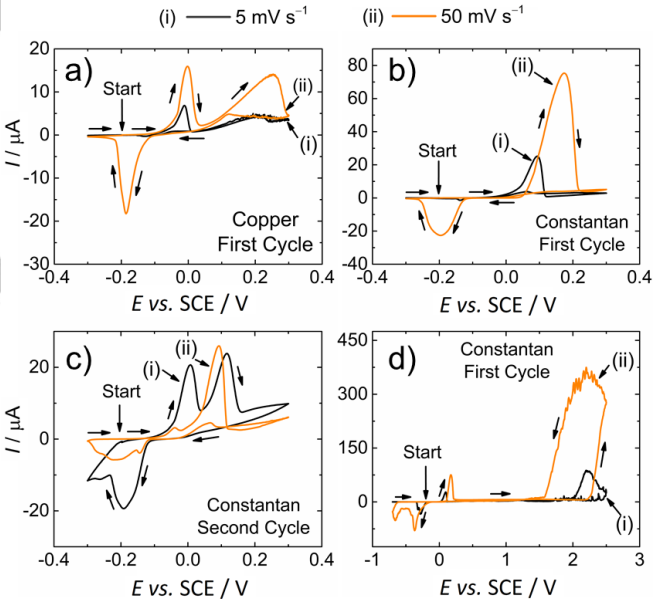

Figure 3. *Cyclic voltammograms at room temperature for 125 µm diameter a) copper and b-d) constantan (Cu54Ni45Mn1) electrodes immersed in 0.5 M NaCl(aq) from open circuit to a-c) +0.3 vs. SCE and d) to +3.0 vs. SCE. Scan rates performed at i) 5 mV s^{-1} (black line) and ii) 50 mV s^{-1} (orange line).*

Ni(IV) has been proposed previously to form as poorly defined NiO_2, consistent with Pourbaix diagrams for nickel in acidic aqueous environments at approx. 1.7 V *vs.* SCE (see Figure 1e).[37,43]. NiO_2 has been suggested as an oxidant,[44] both as a stoichiometric oxidant,[45] and nonstoichiometric oxidant for a variety of organic compounds.[46] NiO_2 in contact with water is

known to decompose to Ni^{2+} and oxygen gas (see equation 3).[45] It is therefore suggested that the formation of oxygen gas at the interface leads to the faster breakdown of the CuCl layer, thus resulting in much higher currents. Gas evolution can be observed experimentally at potentials ≥ 1.7 V *vs.* SCE. However, could this gas evolution be stoichiometric rather than electrocatalytic in nature?

$$NiO_2(s) + H_2O(l) \rightleftharpoons Ni^{2+}(aq) + ½O_2(g) + 2OH^-(aq) \quad \textbf{(3)}$$

Chronoamperometry was employed in order to further investigate the potential dependence of the current noise (Figure 4). Pure copper, constantan, and pure nickel 125 µm diameter electrodes were investigated at 1 V *vs.* SCE (in the passive regions) and at 5 V *vs.* SCE (in the breakdown region). Pure copper exhibited similar currents at 1 V and 5 V *vs.* SCE between 1-50 µA. For constantan, however, lower noisy currents were observed at 1 V *vs.* SCE (1-10 µA), and high currents in the mA range were observed at 5 V *vs.* SCE, confirming the potential dependence of the high current noise for constantan. Current noise for both constantan and pure copper is observed consistently at 1 V and 5 V *vs.* SCE. Pure nickel exhibited no current noise and relatively high currents of 50-100 µA at 1 V *vs.* SCE. At 5 V *vs.* SCE, the current for pure nickel increased drastically into the mA range, similar to the case of constantan, and some current noise is observed (possibly linked to gas evolution). This suggests that the high current noise in the mA range is linked to the presence of nickel. The high current noise for constantan ceases after approx. 5 minutes during chronoamperometry at 5 V *vs.* SCE (Figure 4b) possibly due to substantial recession and gas bubbles affecting the progress of the reaction..

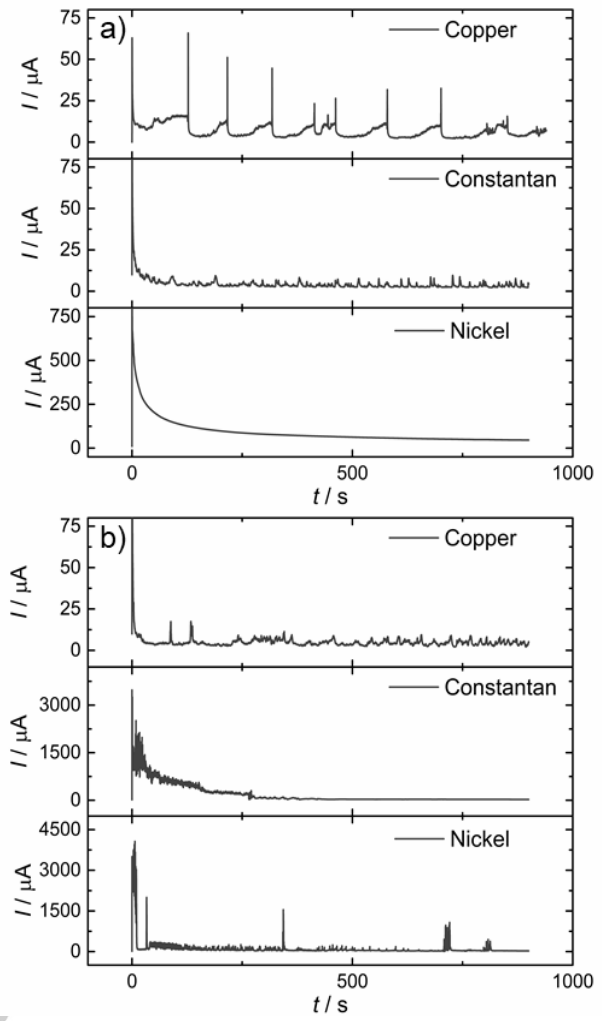

Figure 4. *Chronoamperometric responses for 125 µm diameter pure copper, constantan (Cu54Ni45Mn1), and pure nickel electrodes held at a) 1 V vs. SCE and b) 5 V vs. SCE in 0.5 M NaCl(aq) for 900 s.*

Scanning electron microscopy (SEM) imaging shows that for nickel-containing electrodes, considerable recession is observed compared to observations for copper electrodes. Therefore, the ceasing of high current for constantan could be linked to recession (see Figure 5a1-c1). To explore the presence and role of NiO_2, recession analysis by SEM imaging was conducted for all three types of electrodes (Figure 5a2-c2). Due to the high currents and thus fast recession of the Ni-containing electrodes, 5 V was held only for 2 minutes to allow for sufficient SEM image quality for electrode recession. Since the integral of the *I-t* curve provides charge, the total number of electrons *n* can be estimated from the recission volume. The chemical composition and densities of all three metal electrodes are known. Therefore an estimate for electrode recession can be used to calculate the number of copper and nickel atoms consumed (as well as recession rates, v / µm s^{-1}). Together with *n* and the number of atoms, an estimate for number of electrons given by each copper and nickel atom cna be made. A summary is given in Table 2.

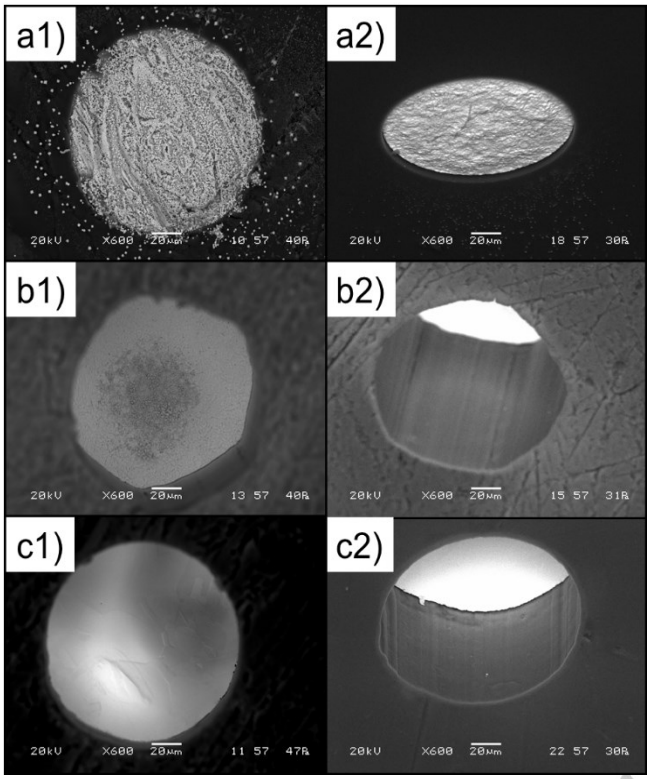

Figure 5. SEM images of 125 µm diameter a) pure copper b) constantan (Cu54Ni45Mn1), and c) pure nickel electrodes after polarisation at +5 V vs. SCE for 2 minutes. 1) flat surface image of an unwashed (film not actively removed) electrode; 2) tilted SEM image for recession estimation after removing corrosion products.

The recession rate estimates show that the nickel-containing electrodes react at least 10× more quickly compared to copper, with constantan giving the highest recession rates at 5 V *vs.* SCE for 2 minutes (0.69 µm s^{-1}). Pure nickel reacts more slowly at 0.48 µm s^{-1}. The number of electrons transferred per copper atom, n_{Cu} for pure copper (Table 2) was assumed to be the same for constantan ($n_{Cu} \approx 1$, equation 1).

Table 2. *Electrode diameter and recession length estimated by SEM imaging, and the number of electrons per Cu and/or Ni atom calculated from chronoamperometric responses for 2 minutes at 5 V vs. SCE in 0.5 M NaCl(aq) at copper, constantan, and nickel 125 µm diameter electrodes.*

Metal	l[a] / µm	v[b] / µm s^{-1}	n_{Cu}[c]	n_{Ni}[d]
Cu	5 ± 2	0.04 ± 0.02	1.0 ± 0.4	-
Cu54Ni45Mn1 (constantan)	83 ± 6	0.69 ± 0.05	1.0 ± 0.4*	7.2 ± 0.7
Ni	57 ± 5	0.48 ± 0.04	-	3.1 ± 0.3

[a] electrode recession measured by SEM imaging, [b] metal recession rate [c] number of electrons per Cu atom (asterisk represents an assumed number of electrons based on previous calculation) [d] number of electrons per Ni atom. Densities used for estimations: copper = 8.92 g cm^{-3}, constantan = 8.93 g cm^{-3} and nickel = 8.91 g cm^{-3}.

The number of electrons per nickel atom, n_{Ni} for constantan was found to be approx. 7 electrons. This estimate is consistent primarily with the stoichiometric formation of Ni^{4+} followed by decomposition to $Ni(OH)_2$ and O_2(g). Some oxygen evolution catalysis due to direct water oxidation is possible, but not a major factor (the number of electrons would be considerably higher). Therefore, it is hypothesised that NiO_2 is forming and acting as a stoichiometric oxidant to release Ni^{2+}(aq) and O_2(g) (equation 2) upon contact to water. Oxide decomposition releasing oxygen is not unheard of. For example, Koper et al.[47] provide evidence for oxygen evolution via oxide decomposition also on gold during anodic polarisation. For pure nickel at 5 V vs. SCE $n_{Ni} < 4$, which indicates predominantly Ni^{4+} formation with some Ni^{2+}.

In an attempt to further investigate the effects of the hypothesised sub-interfacial Ni(IV)/Ni(II) redox switch at 1.7 vs. SCE, the surface of the metal was imaged after cleaning the electrode corroded during chronoamperometry at 1 V (Figure 6a1-c1) and 5 V *vs.* SCE (Figure 6a2-c2) for 2 minutes. The current noise observed for pure copper during voltammetry correspond with the known "pitting potential" region.[48] The SEM images in Figure 6 show evidence for pitting for copper-containing electrodes, which becomes more significant at 5 V *vs.* SCE. For pure copper, the pits are approx. 350 nm in diameter at 5 V *vs.* SCE, whereas for constantan the pits are approx. 450 nm in diameter. Finally, for pure nickel, no pitting is observed at 1 V or at 5 V *vs.* SCE (Figure 6c1-c2). Instead, an etched surface is observed, indicating dissolution of nickel throughout chrono-amperometry at 5 V *vs.* SCE.

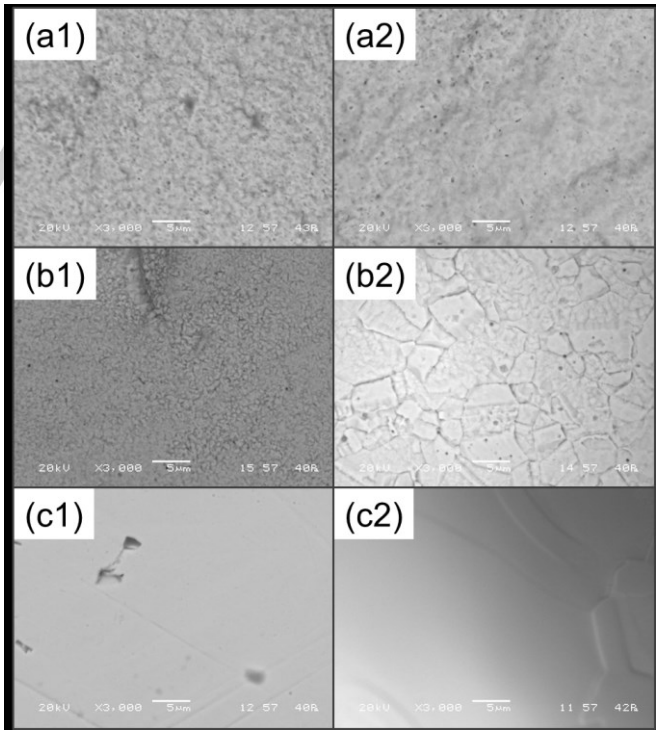

Figure 6. SEM images of 125 µm diameter a) pure copper b) constantan (Cu54Ni45Mn1) Cu-Ni alloy, and c) pure nickel electrodes cleaned after anoic polarisation at (1) +1 vs. SCE for 2 minutes and (2) +5.0 vs. SCE for 2 minutes.

Conclusions

In exploratory work, an underlying interfacial redox mechanism has been proposed for passive film breakdown in two stages for a copper-nickel alloy, constantan, caused by strain at the metal | passive film interface. An initial stage at 0.3 V vs. SCE is linked to the Cu(II/I) redox process leading to low level current noise. The second stage occurs at 1.7 V *vs.* SCE. A transition occurs from low currents (5-6 µA) to high currents (up to 500 µA). The second breakdown has been linked to the Ni(IV/II) potential consistent with the nickel Pourbaix diagram. At 1.7 V *vs.* SCE, NiO_2 is suggested to form at the CuCl | Cu54Ni45Mn1 interface. When exposed to water, NiO_2 acts as a stoichiometric oxidant, leading to oxygen evolution, Ni^{2+} release, and locally acidic conditions at the rapidly corroding interface. The role of NiO_2 as a stoichiometric oxidant was confirmed by calculating the number of electrons transferred per nickel atom, measured by SEM recession analyses. The number of electrons estimated per nickel atom for constantan corrosion was approx. 7, indicating predominantly stoichiometric oxygen evolution.

More work will be required to further unravel these processes. A wider range of CuNi alloys could be investigated. The possible role of Mn in the constantan has not been addressed. The effects of chloride on the Pourbaix diagram also could be considered in more detail[50] to make the prediction of sub-interfacial redox events more reliable. It could be interesting to investigate this passive film breakdown in natural seawater environments. Crousier and Beccaria[10] showed that the corrosion of copper-nickel alloys and copper differs between synthetic seawater and natural seawater. Pure copper and copper-nickel alloys exhibit better corrosion resistance in synthetic seawater. The possibility to perform voltammetric analysis at the sub-interfacial reactive metal | passive film interface could also be of interest for a wider range of metal and metal-alloy systems.

Experimental Section

Electrode Fabrication

125 µm diameter pure copper, pure nickel, and constantan (Cu54Ni45Mn1) wire (ADVENT Ltd. UK) were used to make electrodes. The metal wire was immobilised in a glass tube (~5 mm external diameter; ~5 cm length) filled with a 10:1 wt% transparent epoxy resin (PRESI MA2+ Resin):catalyst (PRESI 100 CC). Silicone tubing was used to extend the resin beyond the end of the glass tube.[34] This allows for re-use of the electrode by back-polishing after recession occurred in experiments. The electrode was left to set at room temperature for 12 hours or set at 100 °C for 1 hour. Copper tape (3M) was used to make an electrical contact and the tubing was removed. The electrode was polished with varying grades of sandpaper and finished with an alumina micropolish suspension and microcloth (1 µm and 0.3 µm particle diameter suspensions, Buehler, U.K.).

Electrochemical Techniques & Instrumentation

Voltammetry and chronoamperometry were conducted using a µAutolab Type III potentiostat (Metrohm) with a three-electrode system in 0.5 M NaCl(aq) (Merck, >99,9% pure). The three electrode system consisted of a 125 µm diameter copper, nickel, or constantan copper-nickel alloy working electrode, a saturated calomel reference electrode (SCE) and a platinum wire counter electrode. Linear sweep voltammetry, cyclic voltammetry and chronoamperometry were conducted with freshly polished electrodes within a potential window between equilibrium potentials and +5 V *vs.* SCE. The crystal phase data for metal wires was confirmed by X-ray diffraction (XRD, Bruker AXS D8 Advance diffractometer with a θ-2 θ configuration and using CuKα radiation λ = 1.5418 Å). Electrode surfaces were investigated with scanning electron microscopy (SEM, JEOL SEM6480LV).

Acknowledgements

We thank members of the Department of Chemistry and the Materials Analysis Suite (MC^2) at the University of Bath for ongoing support and access to facilities.

Keywords: Alloys • Breakdown • Anodic Passivation • Marine Corrosion

[1] G. Kear, B. D. Barker, K. R. Stokes, F. C. Walsh, *Corros Sci* **2005**, *47*, 1694–1705.
[2] S. J. Kim, M. Okido, K. M. Moon, *Korean J Chem Eng* **2003**, *20*, 560–565.
[3] J. M. Drugli, U. Steinsmo, S. Valen, in *Mar Corros Stainl Steels* (Ed.: D. Feron), IOM Communications, London, **2001**, pp. 275–282.
[4] S. Liu, C. Chen, L. Chen, H. Zhu, C. Zhang, Y. Wang, *RSC Adv* **2015**, *5*, 98456–98466.
[5] N. Elangovan, A. Srinivasan, S. Pugalmani, N. Rajendiran, N. Rajendran, *J Appl Polym Sci* **2017**, *134*, 44937.
[6] L. Vrsalović, S. Gudić, D. Gracić, I. Smoljko, I. Ivanić, M. Kliškić, E. E. Oguzie, *Int J Electrochem Sci* **2018**, *13*, 2102–2117.
[7] V. Annibaldi, A. D. Rooney, C. B. Breslin, *Corros Sci* **2012**, *59*, 179–185.
[8] F. Brizuela, R. Procaccini, S. Ceré, M. Va´zquez, V. Va´zquez, *J Appl Electrochem* **2006**, *36*, 583–590.
[9] J. Kunze, V. Maurice, L. H. Klein, H.-H. Strehblow, P. Marcus, *Corros Sci* **2004**, *46*, 245–264.
[10] J. Crousier, A.-M. Beccaria, *Mater Corros und Korrosion* **1990**, *41*, 185–189.
[11] I. Milosev, M. Metikos-Hukovic, *J Electrochem Soc* **1991**, *138*, 61–67.
[12] A. J. Pearlstein, H. P. Lee, K. Nobe, *J Electrochem Soc* **1985**, *132*, 2159–2165.
[13] H. P. Lee, K. Nobe, A. J. Pearlstein, *J Electrochem Soc* **1985**, *132*, 1031–1037.
[14] M. R. Bassett, J. L. Hudson, *Chem Eng Commun* **1987**, *60*, 145–159.
[15] A. R. Langley, M. Carta, R. Malpass-Evans, N. B. McKeown, J. H. P. Dawes, E. Murphy, F. Marken, *Electrochim Acta* **2018**, *260*, 348–357.
[16] A. V. Benedetti, P. T. A. Sumodjo, K. Nobe, P. L. Cabot, G. W. Proud, *Electrochim Acta* **1995**, *40*, 2657–2668.
[17] B. Kim, S. Kim, H. Kim, *Adv Mater Sci Eng* **2018**, *2018*, 1–13.
[18] J. B. Maylor, *Anti-Corrosion Methods Mater* **1978**, *25*, 3–9.
[19] F. L. LaQue, *J Am Nav Eng* **1941**, *53*, 29–64.
[20] J. Mathiyarasu, N. Palaniswamy, V. S. Muralidharan, *Chem Sci* **2001**, *113*, 63–76.
[21] H. P. Dhar, R. E. White, G. Burnell, L. R. Cornwell, R. B. Griffin, R. Darby, *CORROSION* **1985**, *41*, 317–323.
[22] G. Kear, B. D. Barker, K. Stokes, F. C. Walsh, *J Appl Electrochem* **2004**, *34*, 659–669.

[23] J. Mathiyarasu, N. Palaniswamy, V. S. Muralidharan, *Corros Rev* **2000**, *18*, 65–103.
[24] P. K. Chauhan, H. S. Gadiyar, *Corros Sci* **1985**, *25*, 55–68.
[25] A.-M. Beccaria, J. Crousier, *Br Corros J* **2013**, *24*, 49–52.
[26] R. G. Blundy, M. J. Pryor, *Corros Sci* **1972**, *12*, 65–75.
[27] R. F. North, M. J. Pryor, *Corros Sci* **1970**, *10*, 297–311.
[28] H. P. Dhar, R. E. White, G. Burnell, L. R. Cornwell, R. B. Griffin, R. Darby, *CORROSION* **1985**, *41*, 317–323.
[29] J. W. Schultze, M. M. Lohrengel, *Electrochim Acta* **2000**, *45*, 2499–2513.
[30] S. Ikonopisov, *Electrochim Acta* **1977**, *22*, 1077–1082.
[31] S. Ikonopisov, A. Girginov, M. Machkova, *Electrochim Acta* **1979**, *24*, 451–456.
[32] H. Cesiulis, N. Tsyntsaru, A. Ramanavicius, G. Ragoisha, in *Nanostructures Thin Film Multifunct Appl Technol Prop Devices* (Eds.: I. Tiginyanu, P. Topala, V. Ursaki), Springer, Basel, **2016**, pp. 3–43.
[33] B. I. Onyeachu, E. E. Oguzie, I. C. Ukaga, D. I. Njoku, X. Peng, *Electrochim Acta* **2017**, *35*, 127–136.
[34] A. R. Langley, P. J. Fletcher, J. H. P. Dawes, F. Marken, *J Electroanal Chem* 2020 doi 10.1016/j.jelechem.2019.113589.
[35] J. A. Bardwell, B. MacDougall, *J Electrochem Soc* **1988**, *135*, 2157–2161.
[36] J. A. Bardwell, B. MacDougall, M. J. Graham, *Corros Sci* **1991**, *32*, 139–149.
[37] M. Pourbaix, *Atlas of Electrochemical Equilibrias in Aqueous Solutions*, NACE International, **1974**.
[38] Y. Hosokawa, F. Kajiyama, T. Fukuoka, *Corrosion* **2004**, *60*, 408–413.
[39] R. K. Gupta, M. Y. J. Tan, J. Esquivel, M. Forsyth, *Corrosion* **2016**, *72*, 1243–1251.
[40] G. M. Schmid, *Corrosion* **1982**, *38*, 233–234.
[41] R. O. Y. P. O. Gartland, E. Bardal, R. E. Anderson, Johnsen, *Corrosion* **1984**, *40*, 127–133.
[42] T. Worzyk, in *Submar Power Cables*, **2009**, pp. 9–50.
[43] L.-F. Huang, M. J. Hutchison, R. J. Santucci, J. R. Scully, J. M. Rondinelli, *J Phys Chem C* **2017**, *121*, 9782–9789.
[44] K. Nakagawa, R. Konaka, T. Nakata, *J Org Chem* **1962**, *27*, 1597–1601.
[45] H. Ji, T. Wang, M. Zhang, Y. She, L. Wang, *Appl Catal A Gen* **2005**, *282*, 25–30.
[46] V. George, K. S. Balachandran, *Chem Rev* **1975**, *75*, 491–519.
[47] O. Diaz-Morales, F. Calle-Vallejo, C. de Munck, M. T. M. Koper, *Chem Sci* **2013**, *4*, 2334–2343.
[48] D. Kong, C. Dong, M. Zhao, X. Ni, C. Man, X. Li, *Corros Eng Sci Technol Int J Corros Process Corros Control* **2018**, *53*, 122–130.
[49] S.-J. Kim, S.-J. Lee, S.-O. Chong, *Mater Res Bull* **2014**, *58*, 244–247.
[50] A. M. Alfantazi, T. M. Ahmed, D. Tromans, *Mater Design* **2009**, *30*, 2425–2430.

Entry for the Table of Contents (Please choose one layout)

Layout 1:

ARTICLE

The anodic passivation of copper and the copper-nickel alloy constantan (Cu54Ni45Mn1) are investigated and compared here at high positive overpotentials in 0.5 M NaCl(aq). Abrupt potential-dependent passive film breakdown is observed for the copper-nickel alloy during voltammetry and chrono-amperometry experiments in two stages: at 0.3 V *vs.* SCE due to a Cu(II/I) process and at 1.7 V *vs.* SCE due to a Ni(IV/II) process. A breakdown mechanism is proposed based on sub-interfacial redox processes at the interface of a passive ion conductor and a metallic conductor.

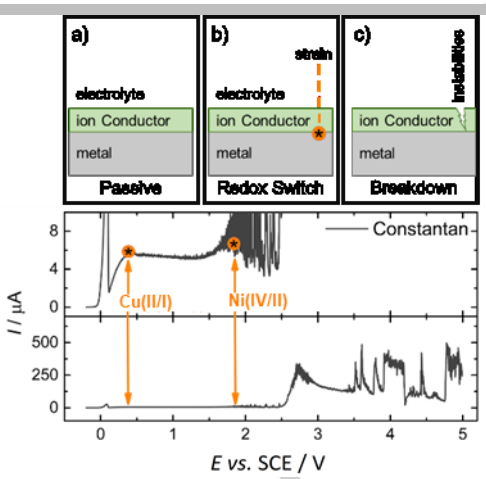

Amelia Rose Langley, Aisling Elmer, Philip J. Fletcher, Frank Marken*

Page No. – Page No.

Linking the Cu(II/I) and the Ni(IV/II) Potentials to Subsequent Passive Film Breakdown for a Cu-Ni Alloy in Aqueous 0.5 M NaCl

Layout 2:

ARTICLE

((Insert TOC Graphic here))

*Author(s), Corresponding Author(s)**

Page No. – Page No.

Title

Text for Table of Contents

Electronic Supporting Information

Linking the Cu(II/I) and the Ni(IV/II) Potentials to Subsequent Passive Film Breakdown for a Cu-Ni Alloy in Aqueous 0.5 M NaCl

Amelia R. Langley,[a]* Aisling Elmer[a], Philip J. Fletcher[b] and Frank Marken[a]*

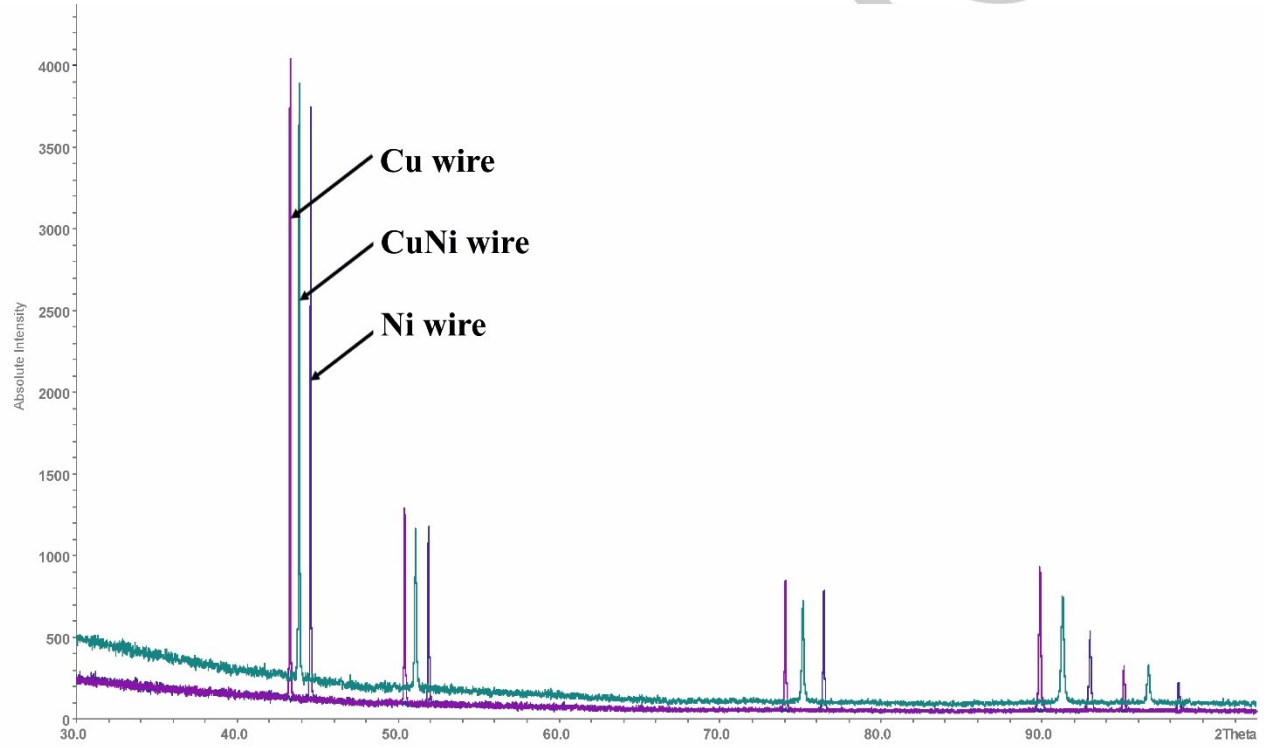

Figure SI1. X-ray diffraction data for copper, nickel, and constantan wire (125 mm diameter) materials employed in electrochemical experiments. The position of the constantan diffraction peaks is consistent with a solid solution alloy with 54% copper.

[a] Amelia R. Langley, Aisling Elmer and Prof. Frank Marken
Department of Chemistry
University of Bath
Claverton Down, Bath BA2 7AY
E-mail: A.R.Langley@bath.ac.uk, F.Marken@bath.ac.uk

[b] Dr. Philip J. Fletcher
Materials and Chemical Characterisation Facility MC^2,
University of Bath
Claverton Down, Bath BA2 7AY